DELFT UNIVERSITY OF TECHNOLOGY

MSC SUSTAINABLE ENERGY TECHNOLOGY THESIS

HOBIT PROJECT - ISC KONSTANZ

Process development of TOPCon rear junction n-type solar cells

OPTIMIZATION OF P+ POLYSILICON REAR EMITTER AND SELECTIVE N+ FRONT SURFACE FIELD

Author :

Sebastian Veerman (4542576)

September 21, 2023

ACKNOWLEDGEMENTS

I would like to express great gratitude towards Dr. Valentin Mihailetchi for making the internship possible and for helping me during my internship, even until the last possible moment. Always making time to discuss the experiments, doing so teaching me a lot. Besides that I enjoyed having a lot of common interests a part from PV Technology, from skiing together to maybe playing football in the future, if my knee is recovered.

I would like to really thank Vaibhav Kuruganti for the pleasant and fun work environment at our office. I'm beyond gratefull for all the help. Helping me with the day to day supervision and supporting me through-out my thesis. I enjoyed working together a lot, without Vaibhav's help this thesis would not have been possible. Always in for a laugh and never passing on the stress of writing a PhD himself.

I would like to thank all the colleagues at ISC-Konstanz for creating a healthy and open work environment. Everybody was always eager to help and explain while conducting my thesis.

I would like to specially thank Prof. Dr. Olindo Isabella for making the internship at ISC-Konstanz possible. Setting me up with Valentin, being always helpful and quick to reply.

At last I would like to thank all the people who made my stay in Konstanz amazing. My new friends, who were open and welcoming. My parents, Fred and Jana, and sister, Julka, for always supporting me from a distance, and the biggest factor of my happiness in Konstanz, Chiara.

Sebastian Veerman

ABSTRACT

Global warming is currently being regarded as one of the most significant concerns in society. As global warming is related to the greenhouse gases emitted from the current energy supply, there is a need for renewable energy sources. Solar energy is an energy source which has zero emissions and could in theory supply the energy demand. A solar cell is technology based on the photovoltaic effect, it converts solar irradiance, specifically the energy derived from photons, into electrical energy. Over the course of the development of photovoltaic technology, numerous variations of solar cells have been introduced.

By IRTPV, it is anticipated that new and advanced concepts, especially the Tunnel Oxide Passivating Contact (TOPCon) solar cell, will come to dominate the solar market in the coming years. At ISC-Konstanz, the primary objective is to develop solar cells that are feasible for industrial applications. The solar cell under investigation and exploration within the context of this particular thesis is referred to as TOPCon Rear Junction (TOPCon RJ), it differs from the well-documented TOPCon emitter Front Junction (FJ). The notable advantage lies in the fact that by placing the emitter at the RJ, the FSF can be lightly doped, thereby reducing Auger recombination. Another advantage is the possibility of increasing the metal pitch between the fingers, reducing the metal used. Even more, the TOPCon RJ doesn't need the high temperature boron diffusion needed for TOPCon FJ, because of doping during APCVD deposition. Simulation results indicate that TOPCon RJ can achieve at least the same efficiency as TOPCon FJ. The TOPCon solar cell is developed on large area n-type Cz wafers, with a selective n++/n+ FSF of c-Si, a by APCVD inline deposited p+ poly-Si layer and screen printed silver contacts. The inline APCVD has fast processing as a major advantage. A comprehensive description of the TOPCon RJ solar cell structure will be provided. The solar cell's parameters will be elaborated on, in order to characterize it. The report incorporates basic supportive solar physics. Various characterization methods will be expounded upon to offer a more comprehensive understanding of the research methodology.

The research is divided into three parts: the development of the p+ poly-Si rear layer, the development of the n+ c-Si FSF, and the process of metallization. Good passivation for the individual layers were achieved and good contacting as well. However, viable cell results were not yet obtained. The research necessitates substantial further enhancements. Moreover, the presence of defects and damages significantly impacted the outcomes, lowering the reliability.

CONTENTS

List of Figures

LIST OF TABLES

1. INTRODUCTION

Global warming is currently regarded as one of the most crucial topics in society. As a consequence of global warming, the sea level rises and disasters occur more frequently [3]. The emission of greenhouse gasses from fossil energy sources is directly related to global warming. To still supply the global energy demand a switch is needed from fossil energy to renewable energy. Solar energy is an emission-free energy source which shows great promise to supply the demand. In the HOBIT project at ISC-Konstanz research is done to improve the solar energy output of a specific solar cell, by increasing the efficiency.

The objective of the project is to develop a solar cell known as Tunnel Oxide Passivated Contact (TOPCon) with a p+ polysilicon (poly-Si) rear junction (RJ) and a selective n+ diffused front surface field (FSF) on a large area n-type Cz wafers. The novelty lies in creating the p+ poly-Si rear emitter. It is formed in an inline process by an atmospheric pressure chemical vapour deposition (APCVD) of an amorphous silicon (a-Si) layer that is either in-situ or ex-situ boron doped and crystallized. The selective FSF is formed in a diffusion furnace with $POCl_3$ gas and subsequently laser doping. The surface passivation is achieved using silicon nitride (SiN_x) and the metal contacts are applied by screen printing a paste that contains silver. The research done in this thesis report is a part of the starting phase of the HOBIT project and can be divided into three main subjects. First is the poly-Si rear layer, second is the FSF layer and third is the contacting of both these layers. A schematic cross-section of the TOPCon-RJ solar cell with selective FSF contacts is shown in Figure 1.1.

Figure 1.1: TOPCon-RJ structure

1.1. OUTLINE OF THE THESIS

This report is divided into four chapters. The first chapter gives a general introduction, on the goal of the project and the work done during this internship. Furthermore, the structure of the report is discussed. The second chapter contains background information on the project. It provides a brief historical context and gives insight into significant solar cell technologies. Subsequently, the TOPCon-RJ solar cell is elaborated, and the main solar parameters are given. Lastly, characterization and process steps are discussed in this chapter. In Chapter 3 the research done is described. The research can be divided into three sections: The front layer, the rear layer, and the contact of both these layers. After each sub-section, the results and outcome of the experiments are discussed. Finally, in Chapter 4 the conclusions and outlook of this work are presented.

2. BACKGROUND

Solar energy technology in general, can be thermal or photovoltaic. In this project only photovoltaic technology is considered relevant. In photovoltaic technology the energy of photons from solar irradiance is converted into electrical energy. These photons are absorbed by technology known as solar cells, which have this capability to transform photon energy into usable electrical power. The focus of this chapter lies in providing a comprehensive background on solar cell's in general and an understanding of the TOPCon-RJ solar cell.

First a brief history and progress in photovoltaics is given, followed by an overview of the solar cell's currently in use and their main characteristics. Explaining the rationale behind the decision for research into the TOPCon RJ solar cell. Subsequently, the TOPCon RJ solar cell is explained in more detail. Elaborating on the structure by going over each of the layers. Next the parameters to characterize the solar cell are discussed. This discussion is complemented by fundamental principles of photovoltaic physics, which establishes the significance of these parameters in characterizing a solar cell. Once the solar parameters have been covered, the characterization methods are explained. This provides further insight into the methodology of the research, as well as the operational aspects of the measurement techniques used to gather relevant information. Lastly, some important process steps are discussed, where numerous alterations occurred during the course of the research.

2.1. TYPES OF SOLAR CELLS AND FUNDAMENTAL WORKING PRINCIPLE

Photovoltaic technology is to the conversion of photon energy into electrical energy, as previously mentioned. This process takes place within specific materials known as semiconductors. The term "semiconductor" is derived from the fact that these materials possess insulating properties in the absence of external energy, but exhibit conducting behavior when external energy is present. This behavior arises because the outer electrons within semiconductors are relatively weakly bound to the core. In semiconductors these outer electrons can be freed by photon energy, resulting in the generation of an electron-hole pair. Electrons and holes are both defined as charge carriers. The term "hole" denotes the absence of an electron, and in contrast to electrons' negative charge, holes possess a positive charge. The electron and hole separate, with the electron moving in the desired direction, a transfer of charge occurs, which is electrical current by definition. Voltage, also known as electric potential difference, is the quantification of the potential energy carried by electric charges, specifically electrons. This potential energy is transferred from photons to electrons through interactions. In fundamental principles of physics, the combination of electric current and voltage yields electric power, and power over time is energy. On this fundament solar cell's generate electrical energy from solar energy.

Since the introduction of the first solar cell in 1883 [4], a multitude of diverse solar cell types and novel concepts have continued to emerge. The classification of solar cells can be categorized into generations. The four generations solar cell's are the, first, second, third and fourth [5]. An overview is given in table 2.1.

Generation	type solar cell
First	Si (mono crystalline) Si (multi crystalline) GaAs
Second (Thin films)	Silicon (amourphous) CdTe CIGS
Third	Multi Junction Dye sensitised Perovskite Organic Quantum dot
Fourth	Hybrid organic with polymer

Table 2.1: Generations of solar cell's

Mostly, first and second generations solar cell's are utilized for commercial purposes. The concepts of the third and fourth generations show promise, but are still in the early stages of research and are not yet market-ready. In the solar cell domain another distinction can be made in the cell's materials. Among all materials, silicon-based solar cells dominate the market, accounting for a substantial market share of 95% [6]. This is due to a combination of high efficiency, easy processing, stability, and cost-effectiveness for silicon solar cell's.

Further distinction in silicon can be made based on the allotropy of the silicon atom. For the solar cell application discussed in this thesis, there are significant structures: mono crystalline, poly crystalline, and amorphous silicon. In mono crystalline silicon, the atoms are arranged in one orientation and form a single crystal. In poly crystalline silicon, the crystals vary in orientation, whereas in amorphous silicon, no crystal order is observed. The most commonly employed form in solar energy is mono crystalline silicon, as it represents the purest manifestation of silicon and yields the highest efficiency.

To comprehend the working principle behind silicon solar cell's, the p-n junction is introduced. It is this very principle that is utilized in all subsequently discussed silicon solar cells. In the context of silicon cells, impurities are deliberately added into the silicon layers. When combined with silicon, these impurities result in an excess or deficit of electrons (or holes) within the silicon material. This process called doping, where an excess of electrons is referred to as n-type (negative charge of excess electrons), and a deficit is of electrons referred to as p-type (positive charge of excess holes). When the p- and n-type silicon are combined, a p-n junction is formed. At the p-n junction the electrons from the n-type diffuse towards the p-type, while the holes from the p-type diffuse towards the n-type. Because of this, an electric field emerges, inducing an internal voltage over p-n junction. The importance of this electric field is that it acts as a separation mechanism of electrons and holes, directing them to the desired contacts. That is, electrons toward the n-type side and n-contact, holes towards the p-type side and p-contact.

In new advanced solar cell concepts combinations of mono crystalline (c-Si) with poly crystalline (poly-Si) or amorphous (a-Si) silicon are employed. These advanced solar cell concepts are expected to be utilized in commercial solar panels in the forthcoming years [7]. In order to obtain a comprehensive understanding of solar cells from the past to the future, a brief historical overview is provided. Examples of old solar cell concepts include Al-BSF solar cells, which stands for Aluminium Back Surface Field. Currently, the dominant technology is the PERC solar cell, which stands for passivated emitter and rear contact. This technology encompasses various types with different polarities and structures, but the underlying principle remains the same. The next technologies that will emerge in the coming years are IBC, SHJ, and TOPCon. IBC stands for Interdigitated Back Contact. SHJ stands for c-Si with a-Si Silicon Hetero Junction. TOPCon refers to Tunnel Oxide Passivated Contacts.

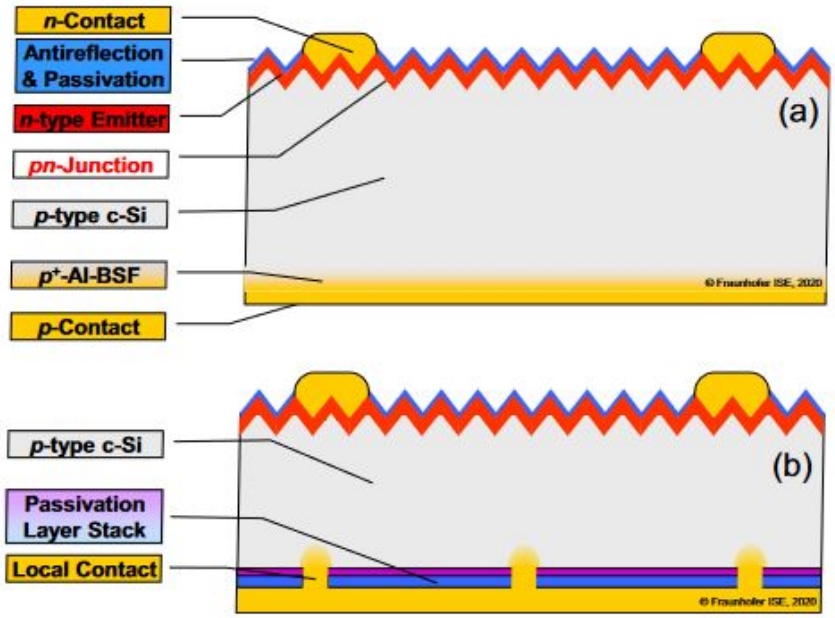

Figure 2.1: a) Al-BSF and b) PERC solar cell structure

In the illustration presented in Figure 2.1, there are depictions of two distinct structures: a) the aluminium back surface field (Al-BSF) and b) the PERC solar cell. the Al-BSF represents the precursor of the PERC solar cell, Al-BSF held a prominent position in solar cell technology since 1960. Over the course of several decades, the efficiency of the Al-BSF solar cell demonstrated a noticeable increase through careful optimization, particularly as a result of advancements in contact pastes. However, there eventually came a point at which this optimization reached a saturation point of 20%. Around 2013 the PERC technology emerged as a viable solution. The replacement of the BSF by a dielectric layer, reduced the rear recombination significantly [8]. By implementing additional passivation (chapter 2.3.5) techniques and streamlining the manufacturing process, the transition from Al-BSF to the more efficient PERC solar cell became feasible. Subsequently, PERC technology began dominating the photovoltaic (PV) market and has continued to maintain its leading position up until the present time. [9].

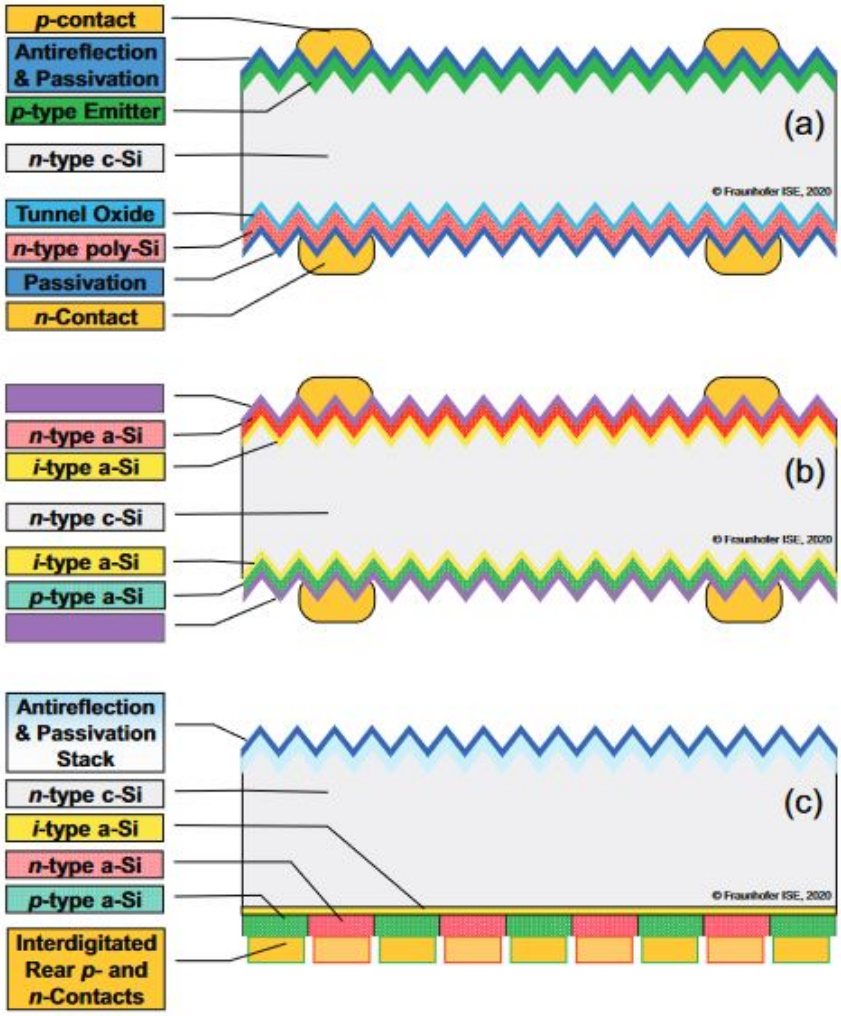

Figure 2.2: a) TOPCon, b) SHJ and c) IBC solar cell structures

The advanced theories upon which the solar cell concepts are founded are diverse and possess their own individual merits. The conventional TOPCon, depicted in Figure 2.2a bears resemblance to the perc, albeit with a reversed polarity. It consists out of a n-type base in place of a p-type base, as well as a p-type emitter instead of a n-type emitter. The enhancement arises from the implementation of a tunnel oxide in conjunction with n-type poly-Si, where the layer provide passivation by conducting electrons and blocking holes. In the case of the SHJ, Figure 2.2b, the heterojunction between a-Si and c-Si possesses differing bandgaps, thereby also affording selectivity for electrons while simultaneously obstructing holes. As for IBC, Figure 2.2c, it lacks front contacts, thereby eliminating any shading losses that may arise from such contacts. The record efficiencies of TOPCon, SHJ and IBC solar cell's are 26.4 % [10], 26.81 % [11] and 26.7 % [12] respectively.

Over the past few decades, there has been a noticeable improvement in the overall efficiency of solar cells [13]. It is a well-established fact that the costs of PV technology decrease as the production capacity increases [14]. As the goal is to provide a for industry viable solar cell, it is of importance to align research efforts with the prediction of solar cell production. In the year 2022, p-type Passivated Emitter and Rear Cell (PERC) solar cells dominated the PV market, accounting for approximately 80% of all modules produced [7]. Even though PERC is a matured technology, it is also subject to certain limitations. The anticipated upper limit for PERC technology is approximately 24.5% [15], a thresh hold that is nearly reached. To overcome this limit other technologies are considered. Consequently, alternative technologies are being explored to surpass this limitation. This thesis examines the Tunnel Oxide Passivated Contact (TOPCon) technology, which is expected to gain a significant market share. According to predictions, n-type TOPCon cells are projected to hold a 60% market share by the year 2033 [7]. As illustrated in the Figure 2.3 from the ITRPV report below. The TOPCon cell is similar to PERC in many ways but incorporates additional passivation techniques. The poly silicon layer functions as a passivation layer as well as the emitter layer. The tunnel oxide enhances charge carrier selectivity, reducing recombination and thus increasing efficiency.

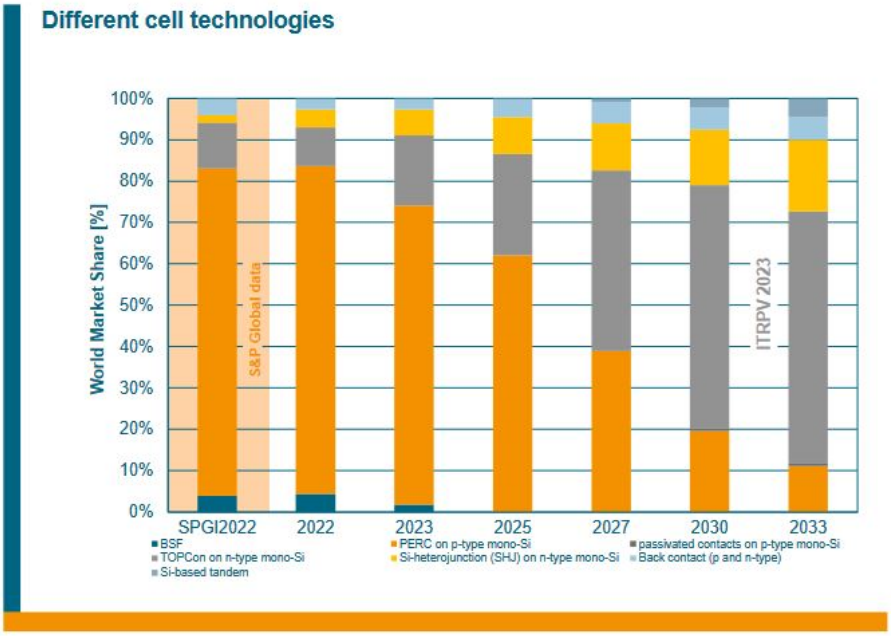

Figure 2.3: prediction of future solar cell technologies market share by ITRPV

2.2. TOPCon solar cells

Normally, when the term TOPCon is mentioned, it typically refers to TOPCon front junction. TOPCon front junction features the emitter positioned on the front side of the solar cell. There is however, also a type called TOPCon rear junction, in which the emitter is situated on the back of the solar cell. In industry, TOPCon front junction is predominantly utilized and extensively researched. However, this technology has its limitations. TOPCon rear junction offers the advantage of a lower doped FSF and consequently reducing Auger recombination. This advantage arises from the fact that the emitter is located on the rear side, as a consequence, there is no need for lateral conductance in the FSF. Furthermore, the n-type FSF is already well-established through the PERC process, allowing for easier implementation. Another advantage over TOPCon FJ is that by using APCVD for poly deposition and doping, the high temperature boron diffusion is not needed, making RJ more cost-effective. In TOPCon FJ the metal pitch is increased, the distance in between the fingers, doing so lowering metal consumption and reducing metal recombination (Figure A.1, appendix). We used Quokka3 three-dimensional simulation tool to model the performance potential of TOPCon front and rear

junction concepts based on experimental input parameters and realistic assumptions. In Figure2.4 the simulation results show that the same efficiency can be reached with rear junction as with front junction.

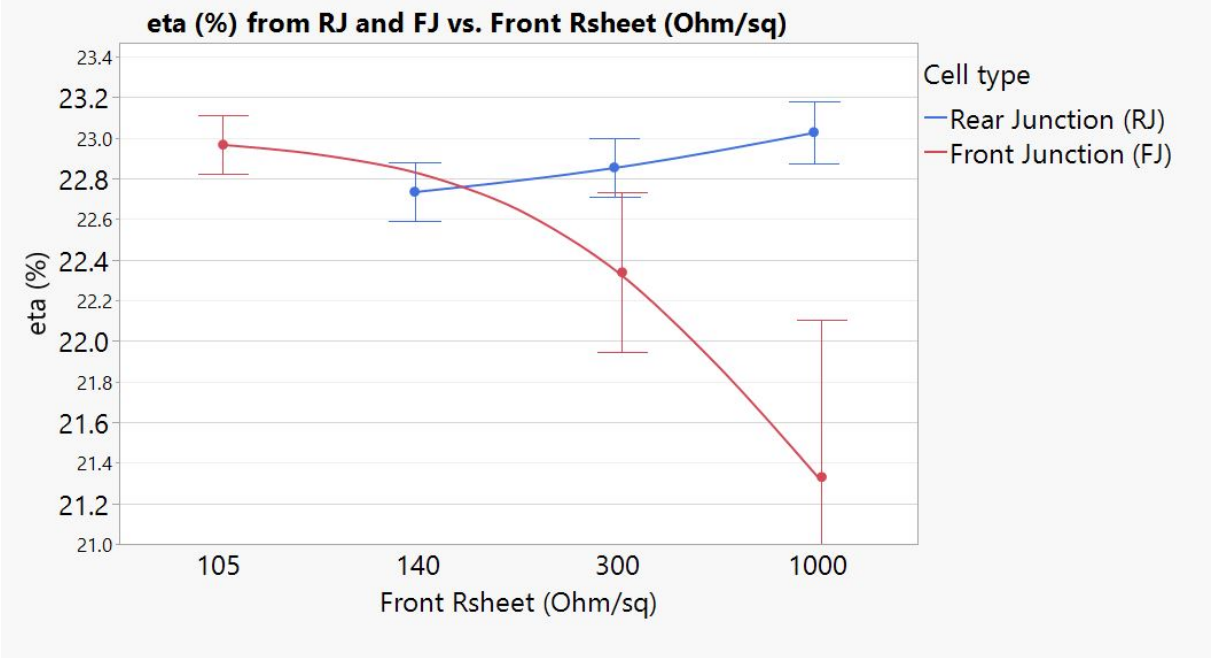

Figure 2.4: Simulated solar cell efficiency (eta) of TOPCon rear junction (RJ) and front junction (FJ) as a function sheet resistance.

2.3. TOPCon RJ in HOBIT project

As previously stated in the introduction, the primary objective of the HOBIT project is to fabricate a commercially viable TOPCon RJ solar cell for the industry. This specific design for solar cells is manufactured on large area n-type Cz wafers. The manufacturing process includes the deposition of a p+ poly-Si rear layer using the inline APCVD technique, as well as the formation of a selective FSF n++/n+ c-Si layer through the use of a diffusion furnace. The research is conducted on Cz wafers with a large surface area. In order to be feasible for industrial application, the solar cell must exhibit high efficiency, employ simple processing steps, and have minimal cost in terms of both money and energy. Desired is to use existing machinery and processing steps, so the manufacturing can be easily implemented by industry.

2.3.1. CELL'S STRUCTURE

THe TOPCon-RJ consists of the following elements from front to back:

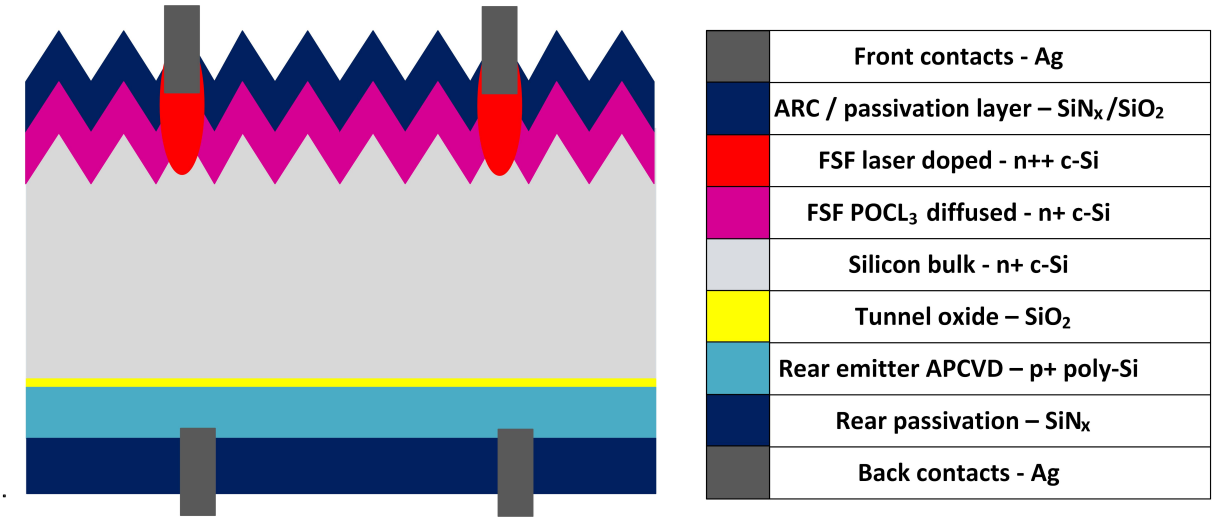

Figure 2.5: TOPCon RJ detailed structure

2.3.1.1 FRONT CONTACTS (AG)

The top parts are the front contacts. In this case the contact are thin screen printed straight lines called fingers made from silver. After the thin fingers thicker busbars (BBs) are printed on top. For the fingers and bus bars it is important they shade the solar cell as little as possible, while still being able to collect and conduct generated electrons in the solar cell. The resistance of the contacts is dependent on the cross section and silver paste of the contact. The higher the cross section the lower the resistance. This means a trade-off has to be made for contact width in respect to shading and resistance. Because the generated current flows through these fingers the resistance has to be as low as possible to minimize losses. To minimize resistance between the contacts and the silicon, a heavily doped n++ by means of laser doping is formed under the contact regions.

2.3.1.2 ARC AND PASSIVATION LAYERS SiN_X AND SiO_2

The first layer is a passivation layer of SiN_x. The contact penetrates through this layer. The layer has multiple functions. It functions as an anti-reflective coating (ARC), as it's desired that the cell reflects as little light as possible. According to optical relations, reflection depends on the refrective indices of the materials travels from and travels to. The refractive index of SiN_x is around 2, which is between air and silicon according to optical relations [16]. Making it a perfect material between air and silicon. The surface is textured, meaning it has a pyramid like surface. The incident light is hereby refracted into the cell so that the waves have a longer path length and increased internal reflection [17]. The SiN_x layer has to be highly transparent and has to have a low absorption, so photons can pass through and generate charge carriers in the silicon layers. SiN_x passivates through field-effect passivation and chemical passivation. Field-effect induces an electric field by fixed charge in the SiN_x. The field-effect reduces recombination by repelling minority charge carriers from the surface [18]. Chemical passivation by decreasing defect states which occur at the Silicon surface [19]. For SiO_2, this of course has to be transparant and have low absorptivity as well. A part from this, the most important passivation is chemical passivation [20]. Because on low doping n-type silicon, SiN_x has good passivation [18], SiO_2 might not be needed. This is one of the structural design options which will be investigated in the experiments. Important to note is that these layers are to passivate the FSF, addressed in the next subsection, and not the contacts. The contacts penetrate through both the layers and are passivated by heavily doped silicon which will be addressed in the second next subsection.

2.3.1.3 FRONT SURFACE FIELD (FSF)

The FSF, front surface field is a passivation layer for the n-type bulk. It works on the field-effect passivation principle. It consists of a phosphorus doped n+ silicon layer. It should repel holes, for this reason the doping should be higher than the bulk but not to high. High doping also means high parasitic absorption. Underneath the contacts the highest doped region is wanted. The highest doping will attract the generated electrons to the front contacts, high doping also means high conductivity and low resistance at the contacts. This follows theory as can be seen in formula's and Figure 2.6.

$$\sigma_n = q * \mu_n * n \tag{2.1}$$

In this σ_n is the conductivity and n the electron concentration, q the electron charge constant and μ_n the electron mobility. When more the electron concentration is high, it increases the conductivity for electrons. An electron get a push from another electron and jump to another atom, here they push away an electron again and so on. This is the movement of electrons in current. this is why more free electrons means better conductivity as there are more loosely bound electron which can be pushed, doing so conducting the current. In the formula's from Neamen, it can be seen that conductance increases with higher electron concentration, thus with higher doping. In the tunneling formula also from Neamen, the relation between high doping and tunneling resistance is shown. [21].

$$R_c = exp\left(\frac{2\sqrt{\epsilon_s * m_n}}{h} * \frac{\phi_B n}{\sqrt{N_D}}\right) \tag{2.2}$$

With at high doping that N_D is (almost) equal to the electron concentration. Figure 2.6 shows the contact resistivity formula in a graph[1]. Again high doping is desired for low contact resistivity.

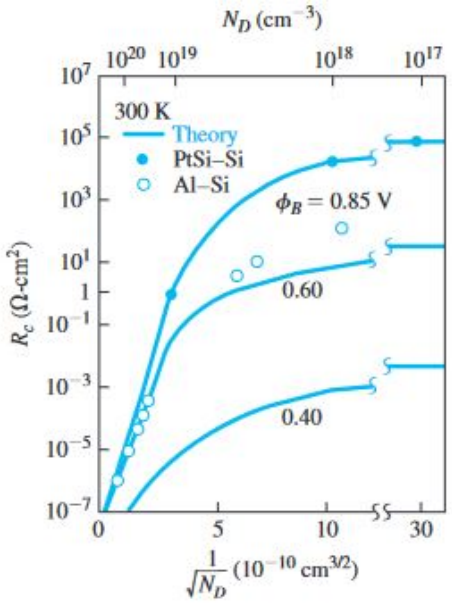

Figure 2.6: Contact resistance vs doping concentration theory [1]

This localized n++ FSF is done by laser doping the n+ FSF layer. By lasering the wafer phosphorous atoms from the PSG are driven into the layer, increasing the concentration and concentration depth. The higher doping in the areas beneath the contacts will mean more parasitic absorption but as the areas are mostly shaded by the contacts, the effect is less detrimental.

2.3.1.4 BULK - N-TYPE MONO SILICON

The bulk is the largest layer of the cell, in this case an n-type crystalline silicon wafer. Here most generation happens and the most important parameters are the minority charge carrier lifetime and base resistivity. It functions as the n-side of the p-n junction, which induced the electric field over the solar cell. The importance of the minority charge carriers is derived from the ambi-polar transport equation [22].

2.3.1.5 TUNNEL OXIDE - SiO_2

Between the bulk n-type silicon layer and the emitter p++ poly silicon a tunnel oxide layer is implemented. This is for transferring electrons and holes to the right contacts. Tunnel-oxide blocks electrons moving from the n-side the p-side and lets holes through, the holes will tunnel through this oxide. As most holes are generated on the p-side and most electrons on the n-side of the p-n junction, it means little holes exist at the n-side of the p-n junction.Which again means less recombination. A lot of research has been done already to the thickness of the oxide, it has to be thin. When the oxide is to thick the electrons can't tunnel and the whole principle doesn't work, it would just be an insulation layer. Another important thing about silicon oxide is that it decreases defect states at both the c-Si an poly-Si interfaces. Which decreases SRH recombination and chemically passivates the layers.

2.3.1.6 REAR EMITTER - P+ POLY-SI

The p-n junction in this solar cell, is located at the rear, hence the name rear junction (RJ). The p-type side of the p-n junction is composed out of highly p type doped poly-Si, a crystallized amorphous silicon layer. While the crystals in c-Si possess a singular orientation, poly-Si contains multiple orientations of crystals, hence its name. The deposition process involves initially depositing amorphous silicon using inline APCVD, followed by crystallization through high temperature annealing. The layer is deposited after the tunnel oxide, thanks to this specific solar cell structure. The combination of tunnel-oxide and poly-Si not only provides the desired selectivity but also offers a cost-effective implementation.

2.3.1.7 BACK CONTACT

The contact to the back side p+ poly-Si junction is formed by screen printing and subsequent firing of the paste. However, in later stages of the HOBIT project the poly-Si metallization will be replaced by a screen printed aluminium paste. The important parameters that influence the performance of the solar cell are the metal induced recombination current $J_{0,met}$ and contact resistivity.

2.3.2. SOLAR CELL PARAMETERS

A solar cell's basic parameters are the V_{OC} , I_{SC}, FF and η (efficiency). V_{OC} is the open circuit voltage, which means the highest voltage a solar cell can reach. The open circuit voltage is called this way because this voltage is only reached when the total current is zero, thus an open circuit. The I_{SC} is the short circuit current and this is the highest current the solar cell can reach. This is only reached when the voltage is zero and the cell operates in short circuit. The fill factor is the factor which translates the V_{OC} and I_{SC} to the maximum power a solar cell can reach. As described earlier it is clear that the maximum voltage and current can't be reached simultaneously. So there is a trade-off, a so called maximum power point (MPP). The voltage and current at this MPP are called the MPP-voltage and MPP-current. The fill factor is calculated as follows:

$$FF = \frac{V_{MPP} * I_{MPP}}{I_{SC} * V_{OC}} \tag{2.3}$$

In this thesis there will be mentioned iV_{OC} in characterization, meaning implied V_{OC}. This is an estimated value by measurement devices like QSSPC, this will be discussed later in this chapter. A solar cell's equivalent circuit is given by the single diode equation. This equation is given for a ideal diode, a solar cell is in real life is not an ideal diode [22].

$$I = I_0 \left[exp\left(\frac{q * V}{n * K * T} \right) - 1 \right] \tag{2.4}$$

With in here:
I: current in cell [A]
V: Voltage in cell [V]
q: elementary charge [1.602*10^{-19} C]
n: ideality factor [-]
K: Boltzman constant [1.381*10^{-23} J/K]
T: Temperature [°K]

2.3.3. MAIN RECOMBINATION LOSSES

Another important parameter which influences the efficiency of solar cell is the recombination. Recombination means that the electron and hole pair generated recombine again, by doing so not contributing to the generated current. So recombination can be seen as a loss mechanism. In each part of the solar cell different recombination mechanisms are dominant. Recombination in all parts of the solar cell lowers the total efficiency.
There are three different recombination mechanisms. Radiative, Auger and Shockley-Read-Hall.

Radiative: band to band recombination. Direct recombination of an electron from the conduction band with a hole from the valence band. Doing so radiating a photon. Because Silicon is an indirect bandgap material this recombination mechanism is very low in respect to other recombination.

Auger: With Auger recombination there are three particles, an electron and hole recombine and their energy is given to a second electron.

Shockley-Read-Hall (SRH): This recombination involves defects in the lattice, creating trap states in the bandgap. An electron or hole can exist in these trap states. The SRH recombination increases with more defects in the material.

The recombination current is also addressed as saturation current and abbreviated with J_0. In the characterization of solar cell's most recombination is addressed with the part of the solar cell they're locallized at. So there's bulk recombination, in this case bulk and emitter recombination current are

measured together ($J_{0,base}$). Passivation quality measured by surface recombination ($J_{0,pass}$). Contact quality measured by metal recombination ($J_{0,met}$). This addresses the most important recombination losses in the cell.

2.3.4. Main resistance losses

The most important resistances which characterize the solar cell are the total series resistance and total shunt resistance. The solar cell is affected as can be seen in the following formula [2].

$$I = I_L - I_0 * exp\left[\frac{q(V + I * R_S)}{n * K * T}\right] - \frac{V + I * R_S}{R_P} \tag{2.5}$$

In here the series resistance is abbreviated with R_S and the shunt resistance with R_P. I_L is the light generated current and the losses by R_S and R_P are subtracted to get the actual current in the cell. The equation can be visualised with the following equivalent circuit in Figure 2.7

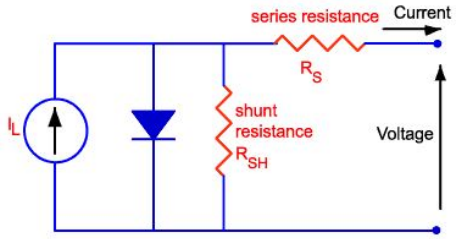

Figure 2.7: One diode equivalent circuit with resistances [2]

The series resistances consist of all the resistance a generated charge experiences. bulk resistance is the resistance of the wafer. The emitter resistance is the resistance of the emitter and should allow lateral conductance, in this case holes. Contact resistance is the resistance in the contact and the resistance between the silicon and metal, in this case the p+ poly-Si emitter and the contact, or between the n++ c-Si FSF and contact. The most dominant resistance losses happen in the contacts and emitter, thus these are needed to be optimized the most. Sheet resistance is used to characterize layers. Because thickness is not always known or homogeneous, it is normalized and given in ohm per square, it is measured at the surface of a layer. For a thin deposited layer, it has to be measured with a polarity difference, as current will otherwise flow through the layer beneath. So for an n-layer sheet resistance, a p-type substrate is needed. It characterizes the electrical properties at the surface of a layer. Shunt resistance is a bit different from the other resistances. Shunting is a loss mechanism where current flows in the wrong direction due to low resistance, kind of short-circuiting the cell partly. So whilst in the previous cases low resistance meant low losses, in this case low shunt resistance means high losses. It can also be seen as the resistance for recombination currents. Shunts occur when impurities connect create a reverse path in the p-n junction. So for example a path for electrons from n region to the p region, with should not happen because of the induced voltage by the junction. All shunts together account for the shunt resistance in the solar cell, abbreviated with R_P.

2.3.5. Passivation mechanisms

Different types of passivation. Two most important are: Chemical passivation and field passivation [23]. Chemical passivation is closing of dangling bonds and decreasing defect states in the lattice. Dangling bonds are "loose" bound electrons located at the end (or surface) of a layer. It exists because the atoms in the lattice structure have these "unconnected" electrons at the outsides. These dangling bonds account for surface recombination. With chemical passivation a thin layer deposited on the silicon binds with the loose electrons. Field passivation is the creation of an electric field to repel

minority charge carriers from the surface, which would otherwise recombine. The electric field can be created by high doping or by certain dielectrics with a fix charge carrier. It is similar to how an electric field is created at a p-n junction. The field passivation also works because of the junction between silicon and another material.

2.4. Processing

A simplified example of the process sequence is given below, of course for each experiment the process sequence was different. The process sequence here is an example of how a TOPCon RJ solar cell would be produced. After this, the most important process steps with which most experiments are done will be discussed in short. There are two routs possible, first n-Si FSF or first tunnel-oxide + poly-Si. As an example the route with first poly-Si emitter is given.

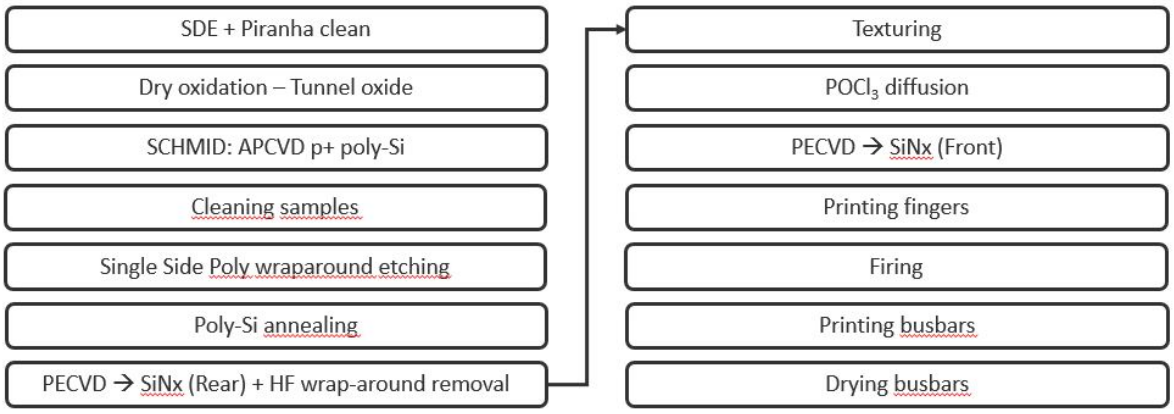

Figure 2.8: Process sequence TOPCon, rear side first

2.4.1. APCVD process

The APCVD process stands for Atmospheric Pressure Chemical Vapor Deposition. APCVD is a deposition with gasses. The gasses are combined in a reaction chamber, where the gasses react and the desired material solidifies on the substrate wafer. In this project an inline APCVD machine is used, meaning wafers are added on a belt and driven through a reaction chamber. In this reaction chamber the desired gasses for a reaction and growth are added, resulting in growth of a layer on top of the wafer. A great advantage from this is the high throughput, which is desired by industry. In this project APCVD is used to form the emitter. The emitter will be a boron doped poly-Si layer. The biggest distinction can be made in in-situ, ex-situ and hybrid doped. In-situ doped is when the boron is added during the a-Si growth, with annealing the layer is therafter partly crystallized to poly-Si. Ex-situ doped is first a-Si growth and then a boron silicate glass (BSG) layer, the boron will be driven in by subsequent annealing whilst also partly crystallizing the layer. Hybrid is a combination of both, doped during deposition and subsequent through a BSG drive-in

2.4.2. Diffusion and laser doping

The diffusion process is based on concentration differences. Higher concentration diffuses to lower concentration. Diffusion is used in a diffusion furnace for this project. It is used to form the phosphorous doped FSF. The process is called $POCl_3$ diffusion. In a high temperature furnace a phosphorous silicate glass (PSG) is grown onto the wafer. During this process the phosphorous diffuses into the wafer, making a shallow doping profile. With a high temperature drive-in the phosphorous is driven deeper into the layer. This high temperature drive-in principle can also be done subsequently in different ways. With annealing or with laser doping. Laser doping is done by using a laser to locally creating high temperature in the wafer. With lasering a certain part can be doped. Hence the name

laser doping. With this the area under the contacts can be laser doped. Creating higher doping in these areas. While the rest of the wafer stays with the same concentration of doping, the concentration from the diffusion. With laser doping the concentration profile changes the depth from shallow to deep, and also increases the surface concentration as well as the general concentration. Here the extra dopant atoms come from the PSG.

2.4.3. Characterization methods

To check and give the quality of the wafers, is called characterization. In this subchapter all of the characterization tools and methods used throughout this study are quickly discussed.

ECV: To check the doping profile of a layer, electrochemical capacitance-voltage profiling (ECV) is used. It is a method where at a chosen point the wafers surface is etched away by a few nm. Whereafter with the capacitance-voltage method, the doping concentration is measured. This repeats itself through out the depth desired. Giving for each depth a concentration and thus a doping profile of doping concentration versus depth in the wafer. ECV measurements are very important and always done for data-analysis. For ECV the wafers can't have any glass on top because the measurement device won't be able to etch and do the measurement.

QSSPC: The quasi-steady-state photo conductance (QSSPC) measurement device gives several parameters of the wafer. The most important is that it shows an implied V_{OC}, $J_{0,pass}$ and lifetime (tau). This is used to characterize the quality of the wafer. In this research a lot of QSSPC data is used. For cell and for layer optimisation. When used for the FSF or emitter layer, symmetrical lifetime samples are used. Symmetrical lifetime samples are as the name suggest symmetrical and to measure the lifetime. As QSSPC measures the total recombination current over the whole layer thickness, the $J_{0,pass}$ is calculated with the known $J_{0,bulk}$. Because it's a total J_0 a single sided sample won't give the correct results. That's why symmetrical samples are used, the $J_{0,pass}$ is then divided by 2 to get the $J_{0,pass}$.

PL: Photo-Luminescence (PL) measurements show the quality of the wafer. It is a laser emitting an IR light in order for the charge carriers to be generated uniformly throughout the bulk of Si. When they recombine, they emit photons. These photons are captured, only the radiative recombination is captured. If other recombination mechanisms are present, there are less photons emitted by radiative recombination, at that point no photons are captures making it a dark point. So with PL the Auger and SRH recombinations or scratches/defects can be visualized. With this a mapping of the cell is done, the more photons radiatively emitted by the wafer the lighter it is visualised. Defects and recombination are clearly visible with this method, however an accurate V_{OC} cannot be taken from this. That's why this measurement can be combined with QSSPC, to give an actual value. With this the rest of the wafer can be quantified with respect to the measured point. On PL metal recombination can be seen clearly, the metallized area will show darker signals. This is used to calculate the $J_{0,met}$ of the contacts. For this samples are used with special printing screens, containing different metal fractions. QSSPC and PL will give lower values, the more metal there is. Total J_0 is derived from QSSPC and PL for each part of the wafer. As the total J_0 will increase with higher metal fractions, because of more area with $J_{0,met}$. With $J_{0,bulk}$ and $J_{0,pass}$ known $J_{0,met}$ can be calculated by fitting it through the several metal fractions.

Ellipsometry: With ellipsometer, the thickness and refractive of a layer can be measured. A wafer is illuminated with a beam of polarized light. The reflected polarized light is captured, after which the tool measures the change in polarization state induced by reflection of the wafer. With this data the thickness and refractive index of a material can be measured by a fitting model [24]. It is used to check if layers have the thickness desired. Also, the homogeneity of layers can be checked by a mapping. The outcome of different deposition, diffusion and etching steps can be checked with this tool.

Four point probe and contact resistance measurements: To measure the sheet resistance and contact resistance a Four Point Probe (4PP) and contact resistance are used. With basic current-voltage relationships, the resistivity is measured and used to characterize sheet resistance and contact resistivity.

For sheet resistance measurements of a layer, it's important to use different polarity substrates. So for the sheet resistance of FSF p-type wafers are used and for the emitter n-type wafers are used. Without the polarity difference, the current through the probes will flow differently and the results will not be accurate.

IV-flasher: To measure the overall cell efficiency. IV measurements are done with an IV-flasher. It measures the current and voltage under Standard Test Conditions (STC), that is an AM1.5 spectrum, 1000 W/m^2 and 25 °C. It uses reference cell's and needs to be calibrated before every measurement. By connected the cell and illuminating it, an I-V curve is measured. Giving all the important parameters needed to characterize the overal solar cell, including V_{OC}, J_{SC}, FF, η, R_{series} and R_{shunt}.

3. Experimental

As mentioned before research can be divided in three main directions, the p+ poly-Si emitter, the n+ FSF and contacting of both regions. In this chapter the research and results are discussed. Each part will first expand about the research, after which the results are given.

3.1. Development of p+ poly-Si emitter

3.1.1. Doping concentration

To obtain the optimal poly-Si layer, various parameters were manipulated. Initially, the impact of dopant concentration on the layer was investigated. The deposition process was carried out using APCVD and was externally performed by SCHMID. The utilization of APCVD, which employs an inline tool, offers significant advantages in terms of rapid processing. In this particular experiment, the poly-Si layer was deposited as a-Si, with boron being added simultaneously during the deposition process, resulting in an in-situ doped layer. Notably, the amount of boron dopant varied during the deposition, allowing for a comparison of multiple dopant concentrations.

Results doping concentration
In Figure 3.1, the impact of the boron doping concentration can be observed. These measurements were conducted using QSSPC. The passivation increases with higher dopant concentration and stabilizes at a dopant concentration of 1.6 wt%. This is evident through the enhanced iV_{OC} and lifetime (Tau) values, as well as the decreased J_0. Important to note is, when the doping concentrations are increased, a borom rich layer (BRL) is formed and the poly-Si layer becomes etch resistance. Consequently, it is unfavorable to have a doping concentration higher than this threshhold. This is due to the fact that a wrap-around of the poly-Si grows at the front side during the deposition process. With an etch resistant layer it is not possible to remove this wrap-around through etching, resulting in contact between the front and back sides, thereby causing a shunt.

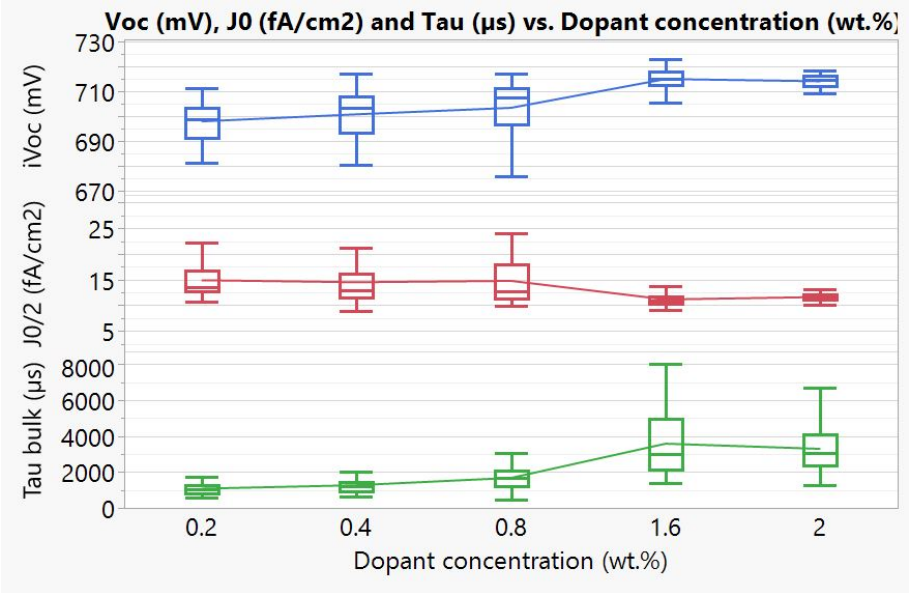

Figure 3.1: Passivation p+ poly-Si for different boron concentrations, given with V_{OC}, J_0 and tau

There remains a need for further optimization of the recipes in conjunction with the etching process. When attempting to utilize solar cells in the experiments, a big challenge was the etching of the poly-Si material. Experiments with creating solar cells were ultimately shunted because of poly-Si wrap-around. An issue here was the comparison between single-side etching and full bath etching, as they do not yield the same etching results. A belt-based single-side etching technique was employed

atop an inline bath, with the top surface being protected by a water capping. In the other case, the wafer was fully etched in a bath, the etching then occurred uniformly and in a more homogeneous manner.

3.1.2. SiN_X CAPPING

There are two process routes which can be selected, beginning with FSF as the first step or beginning with poly-Si as the first step. In the case of initiating with poly-Si, it has to be capped with SiN_x as a protective measure against further processing, such as texturing and $POCl_3$ diffusion. Consequently, the reaction of poly-Si that has been capped with SiN_x during high-temperature annealing was tested. This experiment indicates the behavior of poly-Si when exposed to $POCl_3$ diffusion, a process which entails a high-temperature drive-in step.

Results SiN_x capping
In Figure 3.2, the impact of a SiN_x capping layer on the poly layer is shown. It is obvious that the layer is greatly affected. Measurements were done by QSSPC. When the layer undergoes high-temperature processes with a thick SiN_x layer, a decrease in passivation quality can be seen according to V_{OC}, J_0 and Tau. The presence of a SiN_x capping layer induces stress on the poly-Si layer during high-temperature annealing. This phenomenon occurs due to the different thermal expansion coefficients of the two layers. Another hypothesis revolves around the influence of hydrogen in the poly-Si layer. SiN_x deposition serves as a hydrogen source, and additionally, the presence of SiN_x prevents the escape of hydrogen from the poly-Si layer. Resulting in blistering during annealing [25]. Important to note, in the appendix the firing stability of p+ poly is shown in Figure A.4, the passivation improves after firing, which is needed for contacting.

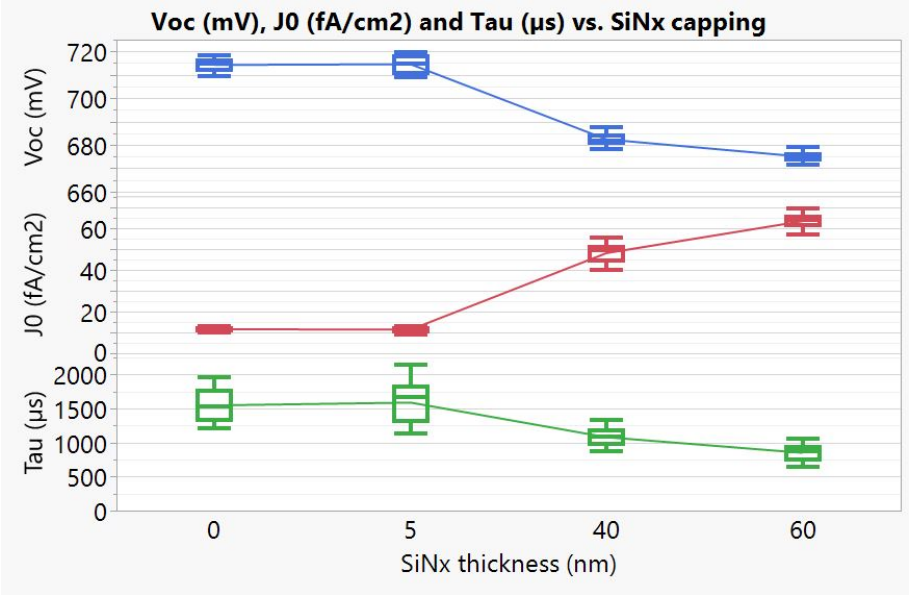

Figure 3.2: Passivation change due to SiN_x capping and subsequent annealing of p+ poly-Si

3.1.3. IN-SITU AND EX-SITU DOPING OF P+ POLY-SI

Another point of investigation for the poly-Si layer involved the consideration of in-situ, ex-situ or hybrid doping. In-situ doping refers to the addition of dopants simultaniously during the a-Si deposition process. On the other hand, ex-situ doping entails the deposition of a BSG layer on top of the first deposited a-Si layer, followed by dopant drive-in during annealing. For hybrid doping, it was both, simultanious doping and a-Si deposition, and further dopant drive-in from a BSG during annealing. The aim was to compare the characteristics of the poly-Si layers that were doped in-situ, ex-situ and hybrid. Additionally, the study explored the concept of hybrid doping, which involves the incorporation of dopants during deposition and subsequent doping through BSG. Due to the

utilization of APCVD for all deposition processes, it was necessary to transport the samples to SCHMID and back, which introduced the potential risk of damaging the cell.

Results in-situ or ex-situ

In figure 3.4, a comparison is made between in-situ, ex-situ, and hybrid doping techniques. It is observed that in-situ doping yields superior values of open-circuit voltage (V_{OC}) , saturation current density (J_0) and lifetime (tau), indicating improved passivation. However, the deposition process of in-situ doped poly involved the layer being deposited in two stages, resulting in two layers stacked on top of each other. Consequently, due to the growth of an oxide layer during deposition, an oxide was present between the layers in this particular case. This occurrence results in a significant increase in series resistance, leading to a decrease in overall cell efficiency (see single diode equation in chapter 2.3.4). A visualization of the oxide between the poly layers is given in Figure 3.3

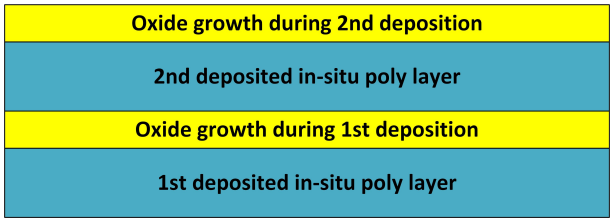

Figure 3.3: Oxide growth in between the poly layers, because of two step deposition

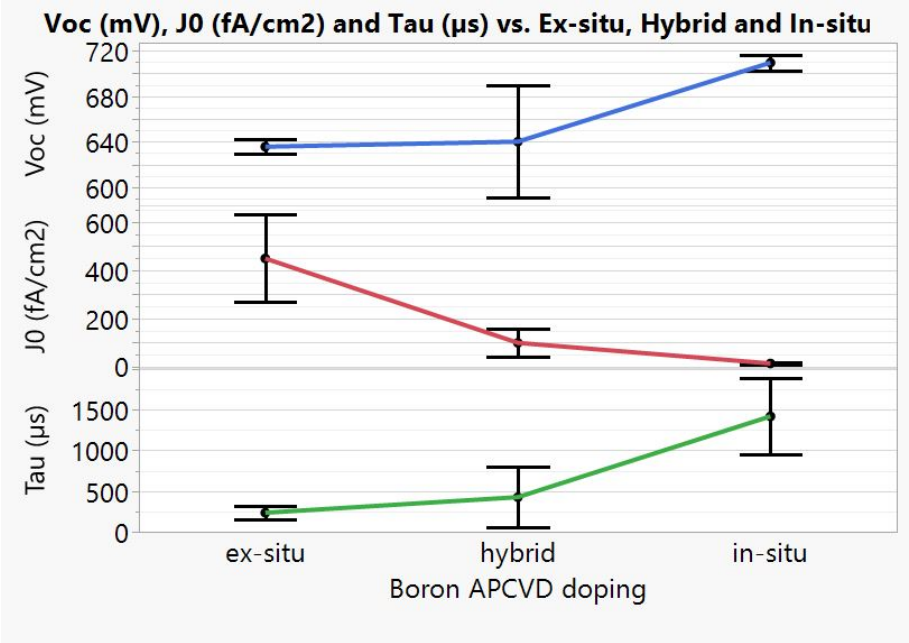

Figure 3.4: Mean passivation parameters of ex-situ, hybrid and in-situ boron doping by APCVD. The error bars represent standard deviation

It is important to acknowledge the fact that comparing the results is challenging due to the presence of processing difficulties. Multiple machines required for the processing procedure after the poly-Si deposition were inoperable. As a consequence the samples had to be stored for several weeks, which, in addition to transportation, resulted in significant damage to the cells. Still, the fact remains that in-situ doped involves a smaller number of process steps compared to ex-situ doped.

3.2. Development of n+ FSF

As mentioned in previous chapters, the FSF entails a heavily phosphorous-doped n-type silicon layer, with a passivation layer of SiN_x or SiO_2/SiN_x on top. The n-type Silicon layer is subjected to local laser doping beneath the contacts to achieve even higher doping at these particular locations. This ensures heightened electron attraction and conductivity within these regions, essentially leading to electron-selective contacts. Due to the TOPCon rear junction nature of the cell rather than the front junction, the FSF layer functions as a passivation layer and not an emitter. Consequently, there is no requirement for lateral conductance, and a greater sheet resistance between the contacts is possible and desired. Doping concentration is inversely proportional to sheet resistance. Lower doping between the contacts is desired, as higher doping also contributes to more Auger recombination. An increase in charge carriers leads to a greater occurrence of the three-particle recombination process, as depicted in the recombination rate formula [22] below.

$$R_{n-Auger} = C_n * N_D^2 * p \tag{3.1}$$

Where C_n is the proportionality constant, N_D is the electron concentration, approximated by donor concentration and p is the hole concentration. According to the formula the electron concentration is squared, consequently meaning, the higher the doping, the higher the recombination rate.

3.2.1. Recipes

Several experiments were conducted to optimize the front surface field. Various diffusion recipes for $POCl_3$ were tested, involving the manipulation of deposition time, gas concentrations, gas flow, temperature, and annealing steps, all of which contribute to the formation of a distinct layer. Altering these parameters leads to changes in different aspects. The depth and concentration of the phosphorous-doped layer vary, as well as the thickness and concentration of the PSG layer, which is grown during the diffusion process. All these parameters were fine-tuned to achieve the desired layer, and a significant amount of prior knowledge on $POCl_3$ diffusion exists due to PERC FSF research. The objective of the hobit project is to attain a high sheet resistance following $POCl_3$ diffusion. Multiple experiments were conducted to optimize the $POCl_3$ diffusion recipes.

Results recipies
In Figure 3.5, the doping profiles of the various $POCl_3$ recipes are shown. To acquire these results ECV measurements were utilized regarding the doping profiles. Accompanying this are the corresponding measurements of sheet resistance obtained through 4PP techniques. Figure 3.6 shows the passivation quality by values for V_{OC}, J_0, and Tau for the same recipes, determined by QSSPC measurements. The sheet resistance values were obtained by implementing $POCl_3$ on a p-type substrate. Would the substrate be of n-type, an accurate measurement of these values could not be achieved. The ECV, V_{OC}, J_0, and Tau values were derived from symmetrical lifetime samples.

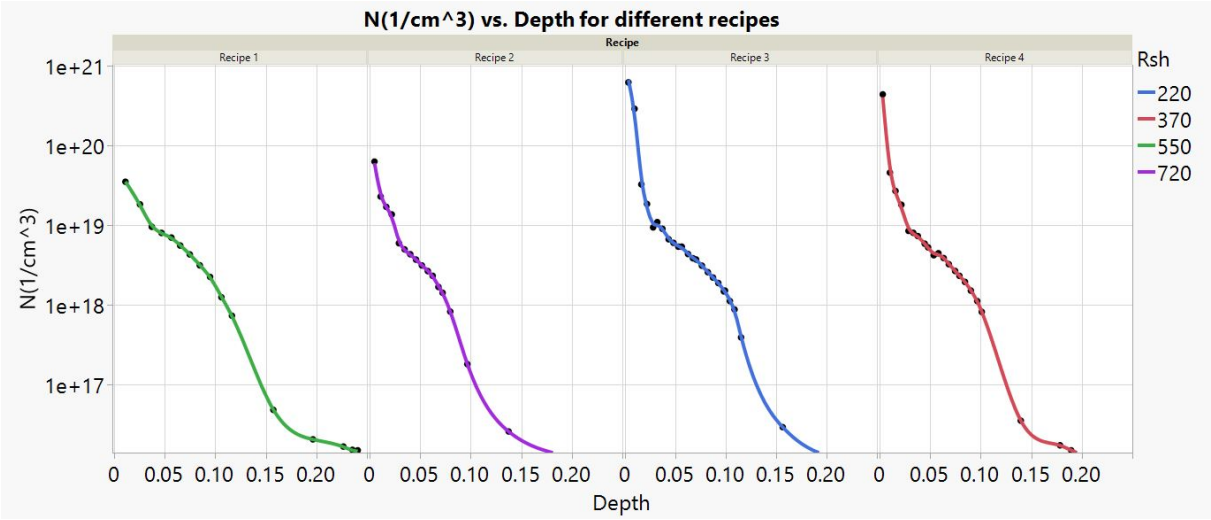

Figure 3.5: ECV-results of different $POCl_3$ recipes, including the sheet resistance

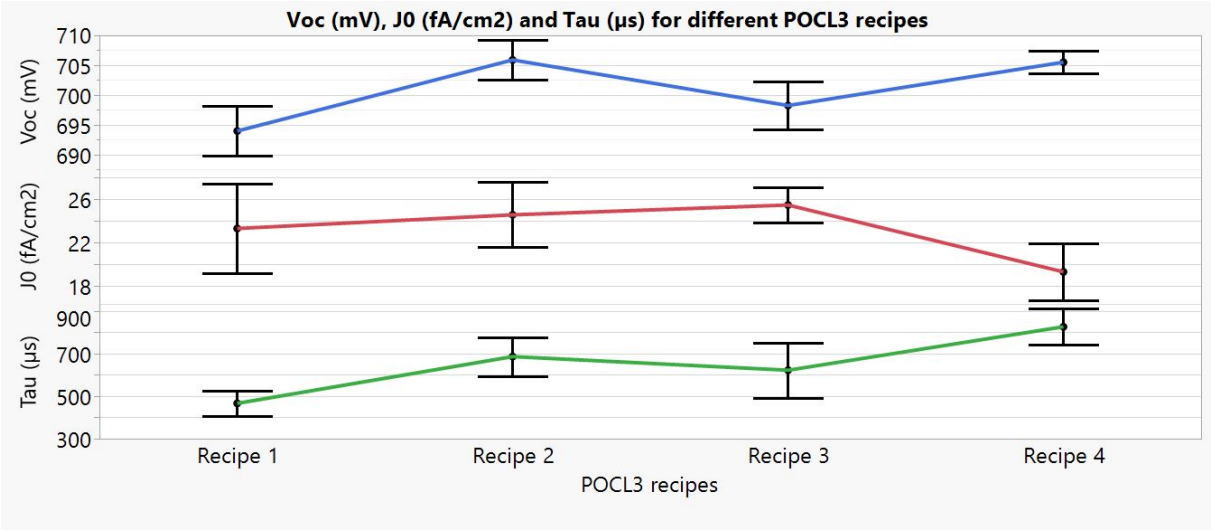

Figure 3.6: V_{OC}, J_0 and tau of different $POCl_3$ recipes

3.2.2. Laser doping

During the diffusion process a PSG layer, containing additional phosphorous, is grown as well. This phosphorous from the PSG layer can be driven into the underlying layer, by using to laser doping. The utilization of laser doping leads to a significant increase in concentration, consequently resulting in a notable decrease in sheet resistance. Various laser fluences and frequencies were experimented with during the laser doping process. However, it was observed that excessively high laser fluence could cause substantial damage to the wafers and a significant reduction in passivation (Figure A.2, appendix). This negative impact is primarily attributed to defects and parasitic absorption, an increase in SRH and Auger recombination, which are consequences of the excessive laser fluence. Moreover, a higher laser fluence implies a greater amount of energy per unit area. In this case, the energy is translated to heat. Similar to high-temperature annealing, this heat facilitates the movement of phosphorous from the PSG layer into the c-Si layer. The use of a laser enables this process to be carried out in a specific and targeted area, which is particularly desirable for the region beneath the contacts. The laser settings had to be made compatible with the contact printing screen and diffusion recipes.

Results laser doping

In figure 3.7 below the doping concentration profile of the FSF is shown after diffusion, measured by ECV. The following laser doping power corresponds to the lines with the sheet resistances in the figure,

measured by 4PP. The figure shows the change in the doping concentration under the influence of laser doping. As can be seen the dopant profiles change with laser fluence, the dopant is driven in deeper with higher laser power. While increasing the laser power from 0 the surface concentration first increases. At 18% laser power the surface concentration reaches a maximum with the tested settings. When increasing the laser power from this point, the surface concentration decreases a little, while the concentration depth keeps increasing. More laser power settings were tested but these three were the most significant: 0% power for reference, 18% for highest surface concentration and 34% for highest power. All laser settings can be found in the Appendix Figure A.3.

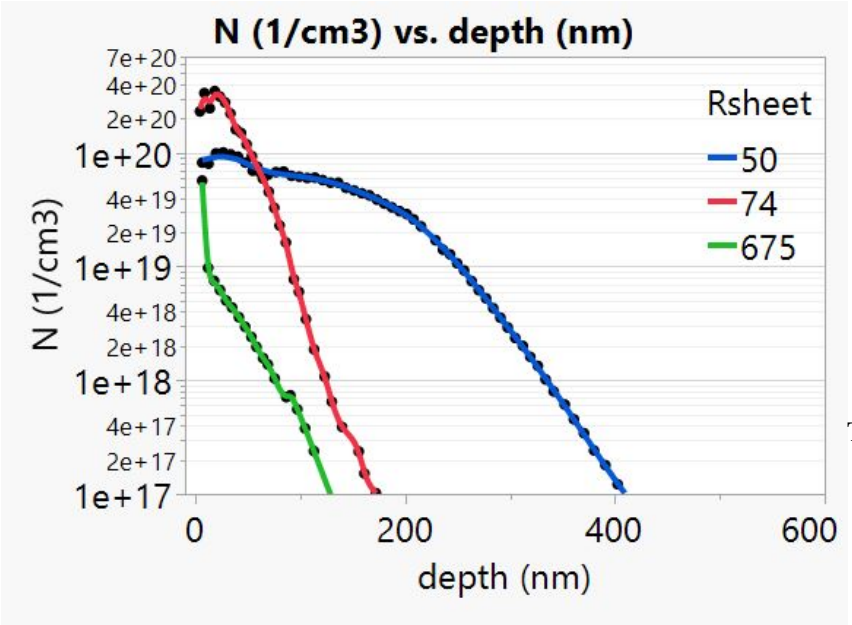

Figure 3.7: ECV of different laser fluence after $POCl_3$ diffusion

Laser power [%]	Rsheet [Ohm/sq]
0	675
18	74
34	50

Table 3.1: Laser power with corresponding sheet resistance

3.2.3. WET-OXIDATION

Additionally, a different strategy is being examined. Based on the findings of the ECV analysis, it indicates that the doping concentration is shallow in depth after the $POCl_3$ diffusion (Figure 3.7. After laser doping the depth of doping increases, along with an increase in surface concentration. It is important to note that for achieving a desired high sheet resistance, the surface doping concentration should not be excessively high after the diffusion process, as seen in previous results (3.7. One potential approach to reduce the surface concentration is through the implementation of wet oxidation. During the oxidation process, a SiO_2 layer is grown on the silicon. While growing it etches away a small fraction (nanometers scale) from the silicon. This etching phenomenon primarily affects the surface of the c-Si FSF, where the doping concentration is at its highest. As a consequence, resulting in a lower (new) surface concentration of the c-Si FSF after oxidation. In addition to the impact of wet oxidation, the influence of the surface passivation stack was investigated in parallel. A comparative analysis was conducted between passivation only by SiN_x, passivation through a stack consisting of SiO_2 (from wet-oxide, thinned to 15 nm) in combination with SiN_x, and passivation involving a stack consisting of SiO_2 (1st SiO_2 removed and re-oxidized 15 nm) along with SiN_x.

Wet-oxidation results

As can be seen in Figure 3.8 the surface concentration lowers, the more oxide is grown during wet-oxidation. Measurements conducted with ECV. This is because more of the highly doped silicon is etched away. With this the sheet resistance increases as expected. The following sheet resistances correspond to the oxide thickness grown in Figure 3.8, sheet resistance measured by 4PP.

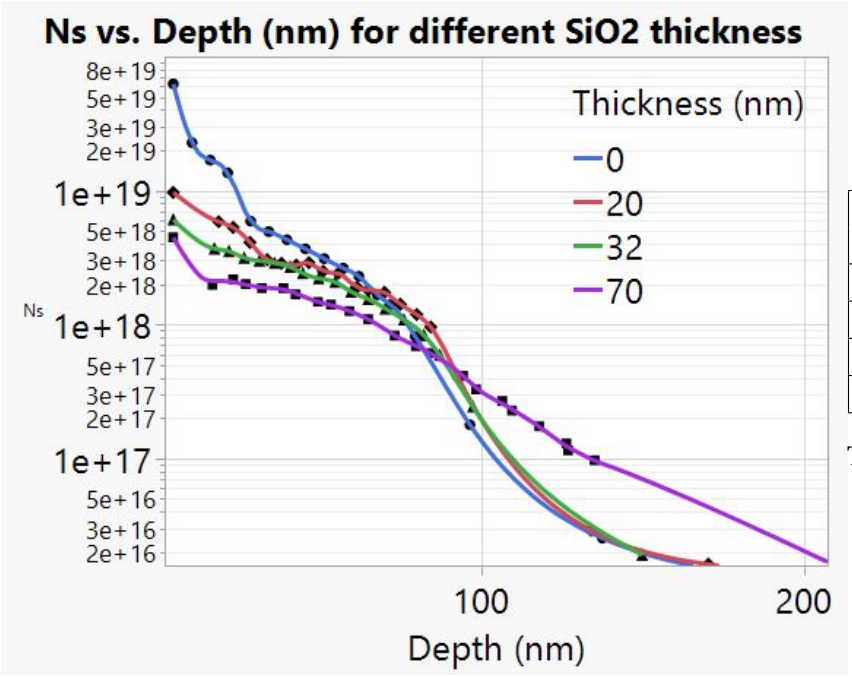

Oxide thickness [nm]	Rsheet [Ohm/sq]
0	720
20	1250
32	1400
70	1700

Table 3.2: Oxide thickness with corresponding sheet resistance of c-Si layer

Figure 3.8: Doping concentration profiles after wet-oxidation

Expected was the V_{OC} to increase, with increasing wet-ox thickness. Because of lower surface doping concentration, expected would be lower Auger recombination. It would follow aforementioned theory and formula's, however, no such trend was observed in this experiment. As can be seen in 3.9, the passivation parameters from QSSPC, V_{OC}, J_0 and Tau do not show improvement for more oxide growth. This might have happened due to damages to the wafers, increasing defects and SRH recombination by increase of trap states. This might have balanced out the lower Auger recombination which was expected.

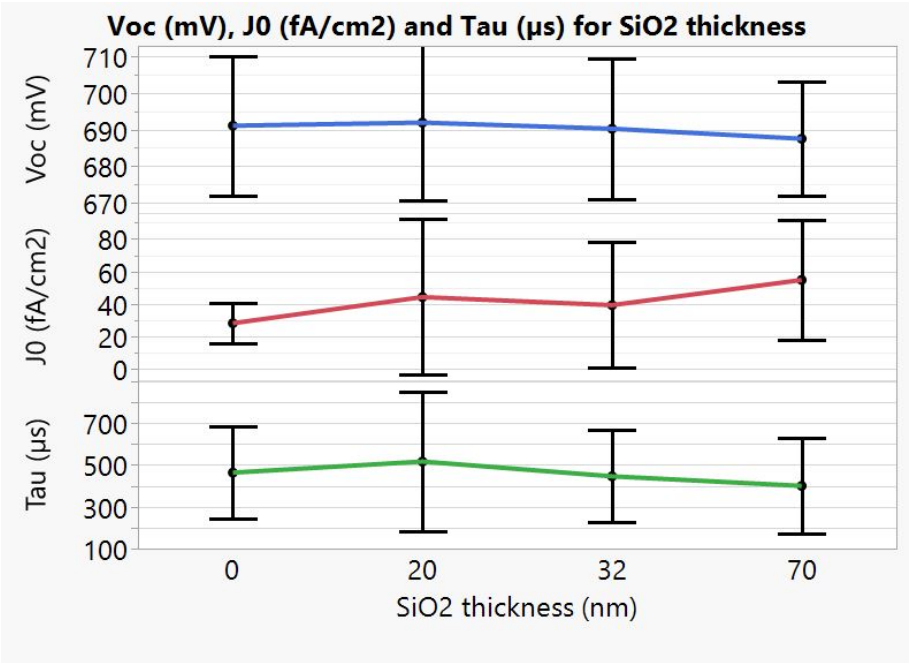

Figure 3.9: Voc, J0 and tau for different wet-oxidation SiO_2 growth

As for the passivation stack the SiO_2/SiN_x stack performs better than just SiN_x layer as passivation. As can be seen in Figure 3.10, passivation parameters from QSSPC show better results for a combined

stack of SiO_2 and SiN_x. There is no significant difference between a thinned SiO_2 and re-oxidized SiO_2, that's why the results of both are combined in the graph.

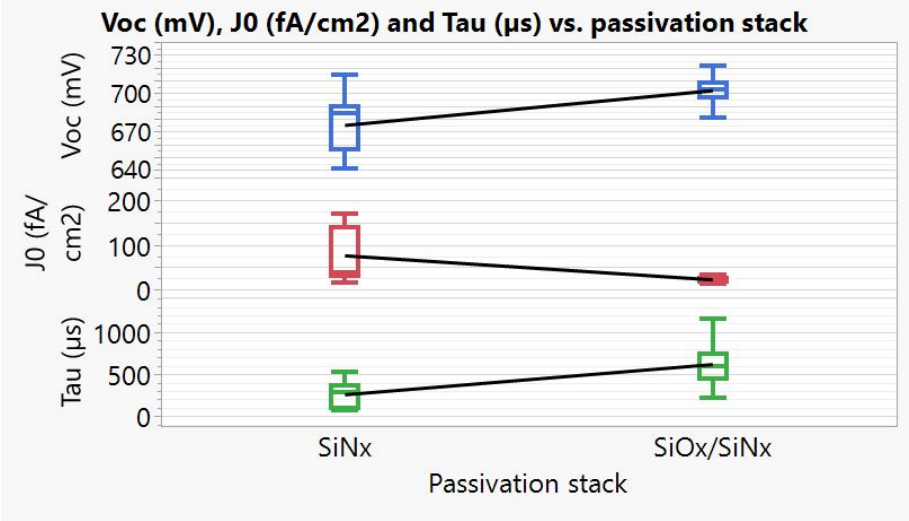

Figure 3.10: Voc, J0 and Tau for different passivation stack

3.3. Metallization

The optimization of the layers is carried out in parallel with the process of contacting, also known as metallization. In order to achieve a high-efficient solar cell, it is necessary to establish a contact with a low contact resistivity. As contact resistivity contributes to the total series resistance and lowers the efficiency of the solar cell. Due to this specific cell structure, there are contacts located at both the front and back. The front contact is created by contacting the highly doped n++ c-Si region of FSF. On the other hand, the contact at the rear or backside of the solar cell is established by contacting the p+ poly-Si emitter layer. It is crucial to optimize the contacts on both sides. The process of contacting involves the use of screen printing, which utilizes a metal grid with gaps through which silver paste is applied. The silver is then deposited onto the wafer through these screens and subsequently dried and fired at high temperatures. This firing process can be conducted at various temperatures and has an impact on the cell's passivation quality as well.

3.3.1. Front contact

For the front contact, as previously discussed, there exists a laser-doped region that must be precisely aligned with the metal. As previously mentioned in chapter 2.3, high doping contributes to a low contact resistivity. In the experiments, the impact of laser doping on contact resistivity is examined and refined. In previous results (Figure 3.7) the high laser power leads to increased doping, which in turn reduces contact resistivity. For different laser power settings the contact resistivity was compared. A further aspect examined was the utilization of different silver pastes.

Results front contact
In Figure 3.11 the influence of laser doping on the contact resistivity is shown. The values show good contact but were achieved with an old laser which is no longer in use.

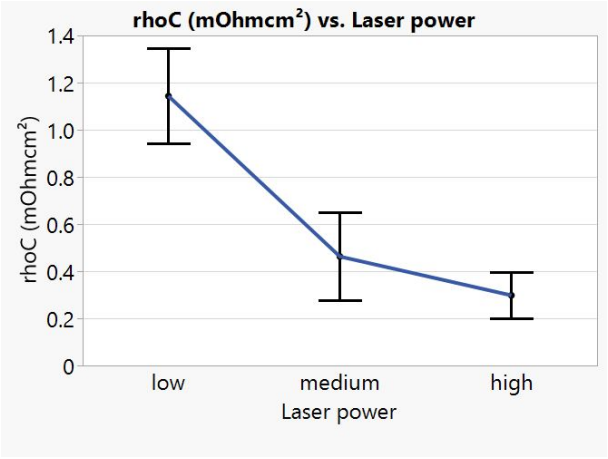

Figure 3.11: Influence laser doping on contact resistivity

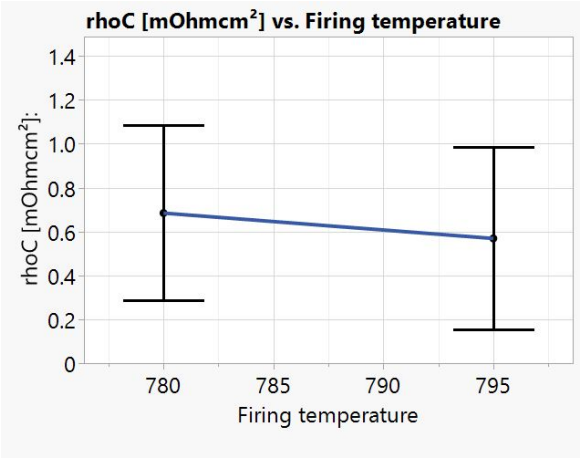

Figure 3.12: Influence firing temperature on contact resistivity

The $J_{0,met}$ values, calculated with different metal fraction wafers. Were good, around 250 fA/cm2. Because of Auger recombination $J_{0,pass}$ increases with higher doping, under the contacts, however this is for small parts and not for the whole wafer. There has to be a trade-off between recombination and contact resistivity. Different silver pastes where tried as well but are not showed here as similar results where achieved and no conclusion as to optimisation could be given. For firing temperature a slight optimization was seen but it is very little as can be seen in Figure 3.12.

3.3.2. Rear contact

Contacting boron-doped poly-Si poses a significant challenge, as screen printing silver paste with lines results in high contact resistivity. Consequently, efficiency is greatly reduced, decreasing the viability of a solar cell for industry . To solve this issue, an alternative approach is tried involves the screen printing of point contacts instead of line contacts. This is an in-house method from ISC and is subjected to confidentiality. This method initially screen prints silver points. After-which the points are connected by a subsequently screen printed silver line, aligned on top of the points. A visual representation of this concept is depicted in Figure 3.13.

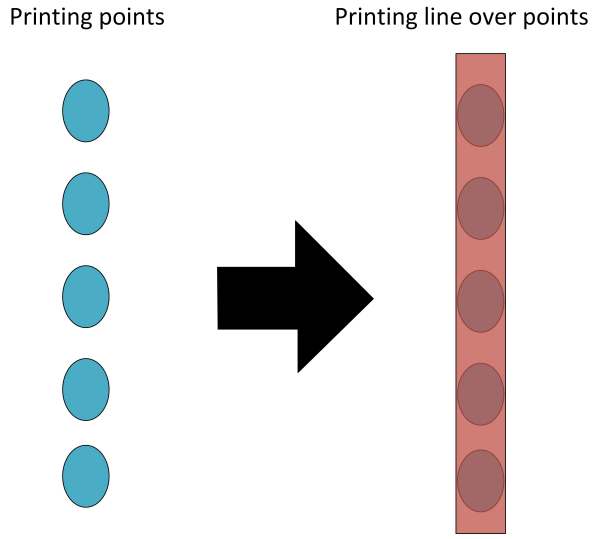

Figure 3.13: Visualisation of screen printing point contacts

Results rear contact

Point contacts show more promising results as can be seen in Figure3.14. There still needs to be done optimisation. Also, with point contacts, it means an extra production step which might not be that

good for industry applications, as it will slow down the process. However, a silverpoint could make aluminium contact easier again. By a combination of silver points and aluminium lines and busbars. It would reduce silver use significantly which is desired as it's a rare and expensive material.

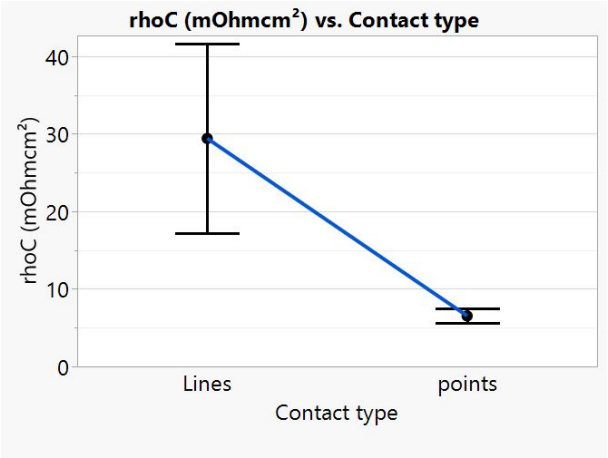

Figure 3.14: Influence of contact type on contact resistivity

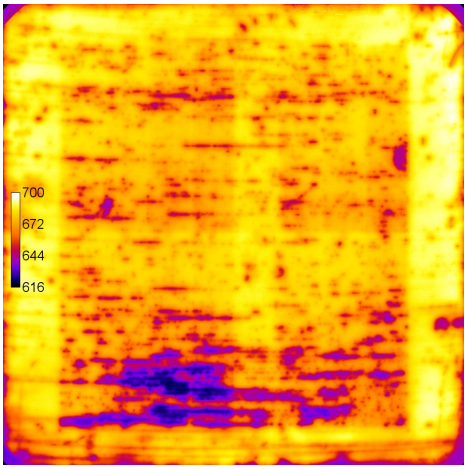

Figure 3.15: Damaged solar cell visualised by PL example

The value of $J_{0,met}$ for the poly contacts was calculated once again, utilizing the identical methodology as previously mentioned. Consequently, a $J_{0,met}$ of approximately 550 fA/cm2 was obtained, which is considered satisfactory for the purpose of establishing contact. However, there is room for improvement on the $J_{0,met}$. It is worth noting that the samples utilized in these experiments exhibited a significant degree of damage, as was seen by the PL images. Therefore, it is possible that the $J_{0,met}$ estimation is not that reliable. An illustration of a damaged $J_{0,met}$ sample is provided in Figure 3.15.

4. Conclusions and Outlook

Conclusion on poly-Si development
The optimal level of dopant concentration required to achieve effective passivation in the in-situ poly-Si layer is approximately 1.6 wt.% (3.1) Despite the expectation that the BRL layer would be etchable at this concentration, the issue of BRL layer formation remains unresolved. In subsequent experiments, it would be advisable to decrease the boron concentration even further. To enhance the conductivity and contact resistivity of the contacts at the rear, it may be worth considering the utilization of local laser doping to activate a greater amount of dopant. By doing so, locally increasing the dopant concentration. Furthermore, the poly-Si layer experiences stress induced by the SiN_x capping. A loss in passivation was observed, depicted in Figure 3.2. Consequently, it would be more advantageous to go for the process flow option of beginning with creating the FSF. By doing so, the poly-Si layer will not be subjected to the high temperature step during $POCl_3$ diffusion, thus maintaining a high level of passivation. The optimal choice for the doping method would be the in-situ doped poly-Si layer. This particular layer exhibited a lower susceptibility to defects and damages, and required fewer process steps compared to the ex-situ or hybrid doped alternatives. The problem of an oxide in between the layers is already fixed, deposition of in-situ will not be done in two steps but in one step in the future experiments, this is already confirmed.

Conclusion on FSF development
For the FSF, the recipy was found for the desired dopant concentration, shallow in depth and low in surface concentration. As a result, the FSF achieved the intended sheet resistance. Moreover, the subsequent laser doping process exhibited great potential, as it substantially increased the dopant depth and surface concentration. Consequently, this led to a reduction in the sheet resistance for the selective FSF under the contacts. However, the wet-oxidation technique did not yet yield the desired outcomes, suggesting the need for further experimentation. On the other hand, the passivation stack comprising SiO_2/SiN_x demonstrated favorable results and can be utilized as a form of passivation, rather than passivation by SiN_x only.

Conclusion on metallization
Good results in terms of front side contact were obtained from the experiments, which were characterized by low contact resistivity and J0,met. This outcome was anticipated due to the advanced state of PERC technology. However, the achieved results were obtained using a laser that is no longer utilized. In order to obtain similar contact results with the new laser, it is necessary to optimize the laser recipe, which requires further experimentation. Regarding the poly-Si layer, effective contact was only achieved through point contacts, which also exhibited low resistivity and J0,met. Nevertheless, there is room for improvement in further optimization, particularly since a reduced boron concentration is necessary to prevent the formation of etch-resistant BRL.

REFERENCES

[1] S. M. SZE and M. K. Lee, "Semiconductor devices," *Physics and Technology*, 1985.

[2] M. A. Green, "Solar cells - operating principles, technology and system applications," *National Library of Australia*, Dec. 1986.

[3] B. R. Singh, "Study of impacts of global warming on climat change: Rise in see level and disaster frequency," *Global Warming: Impacts and Future Perspective*, 2012.

[4] A. Chodos, "April 25, 1954: Bell labs demonstrates the first practical silicon solar cell," *APS News - This Month in Physics History*, Apr. 2009.

[5] J. Pastuszak, "Photovoltaic cell generations and current research directions for their development," *Lublin University of Technology*, Aug. 2022.

[6] Fraunhofer ISE, "Photovoltaics-report," Feb. 2023.

[7] ITRPV, "International technology roadmap for photovoltaic 14th edition," Apr. 2023.

[8] Y. Zhao, "Strategies for realizing high-efficiency silicon heterojunction solar cells," *Solar Energy Materials and Solar Cells*, 2023.

[9] G. M. Wilson, "The 2020 photovoltaic technologies roadmap," *Journal of Physics D: Applied Physics*, May 2020.

[10] Jinkosolar, "Jinkosolar's high-efficiency n-type monocrystalline silicon solar cell sets our new record with maximum conversion efficiency of 26.4," 2022.

[11] H. Lin, M. Yang, X. Ru, G. Wan, S. Yin, F. Peng, C. Hong, M. Qu, J. Lu, L. Fang, C. Han, P. Procel, O. Isabella, P. Gao, Z. Li, and X. Xu, "Silicon heterojunction solar cells with up to 26.81 efficiency achieved by electrically optimized nanocrystalline-silicon hole contact layers," *Nature Energy*, 2023.

[12] K. Yoshikawa, H. Kawasaki, W. Yoshida, T. Irie, K. Konishi, K. Nakano, T. Uto, D. Adachi, M. Kanematsu, H. Uzu, and K. Yamamoto, "Silicon heterojunction solar cell with interdigitated back contacts for a photoconversion efficiency over 26," *Nature Energy*, May 2017.

[13] NREL, "Interactive best research-cell efficiency chart," Sept. 2023.

[14] ITRPV, "Technological roadmap - solar photovoltaic energy, 2014th edition," *IEA agency*, 2014.

[15] V. Shaw, "The weekend read: Life after perc," May 2021.

[16] M. Bron and E. Wolf, "Principles of optics - electromagnetic theory of propagation, interference and diffraction of light," 1975.

[17] S. Mandel, "Pyramid texturing on silicon solar cells traps light more efficiently," *Scilight*, 2020.

[18] H. H. Canar, G. Bektaş, and R. Turan, "On the passivation performance of sinx, sioxny and their stack on c-si wafers for solar cell applications: Correlation with optical, chemical and interface properties," *Solar Energy Materials and Solar Cells*, July 2023.

[19] A. Cuevas and M. J. Kerr, "Passivation of crystalline silicon using silicon nitride," *Photovoltaic Energy Conversion, 2003. Proceedings of 3rd World*, June 2003.

[20] Y. Zhuang, S. Zhong, X. Liang, H. Kang, Z. Li, and W. Shen, "Application of sio2 passivation technique in mass production of silicon solar cells," *Solar Energy Materials and Solar Cells*, May 2019.

[21] D. A. Neamen, "Semiconductor physics and devices," *Physics and Technology*, 2012.

[22] A. H. Smets, K. Jäger, O. Isabella, R. A. van Swaaij, and M. Zeman, "Solar energy - the physics and engineering of photovoltaic conversion, technologies and systems," *UIT Cambrindge, England*, 2015.

[23] S. Chunduri, "Passivation is key for high efficiency solar cells," *TaiyangNews*, May 2021.

[24] J. A. Woollam, "Alpha se - spectroscopic ellipsometer, hardware manual," 2004.

[25] C. Madumelu, Y. Cai, C. Hollemann, R. Peibst, B. Hoex, B. J. Hallam, and A. H. Soeriyadi, "Assessing the stability of p+ and n+ polysilicon passivating contacts with various capping layers on p-type wafers," 2022.

A. APPENDIX

FRONT AND REAR JUNCTION TOPCON COMPARISON WITH METAL PITCH

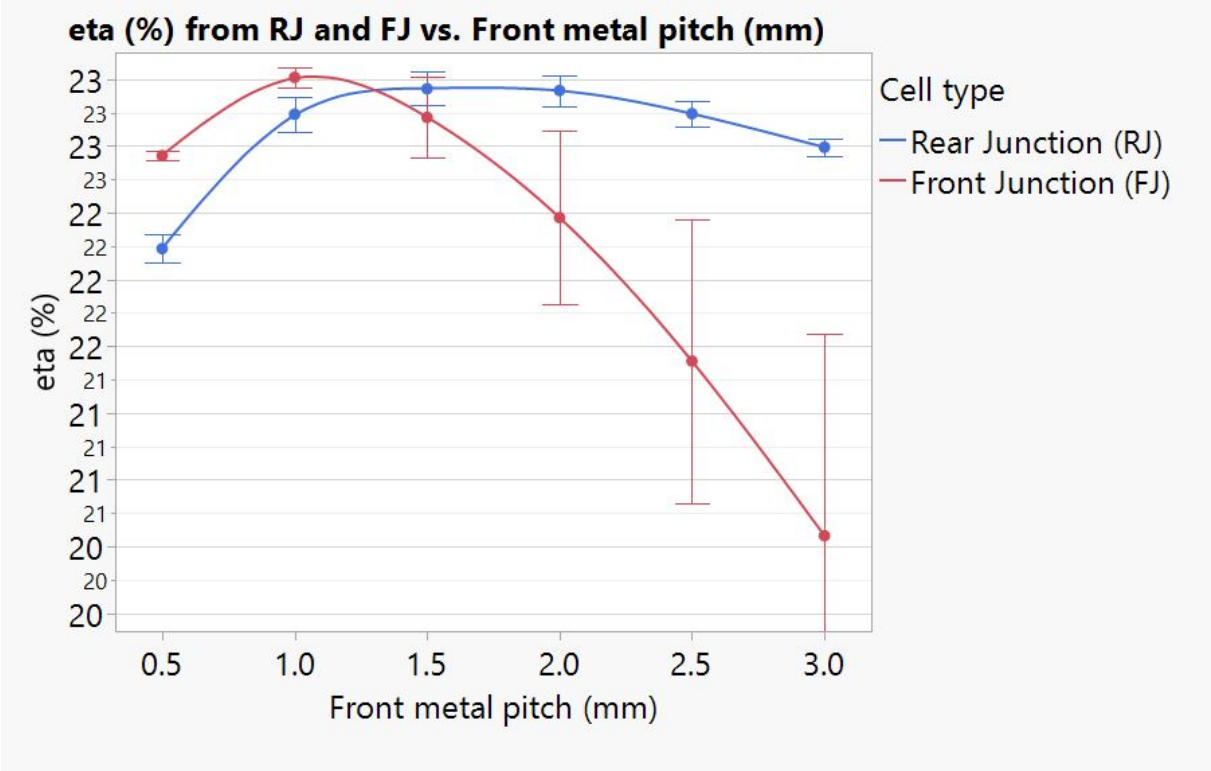

Figure A.1: FJ and RJ TOPCon vs. metal pitch

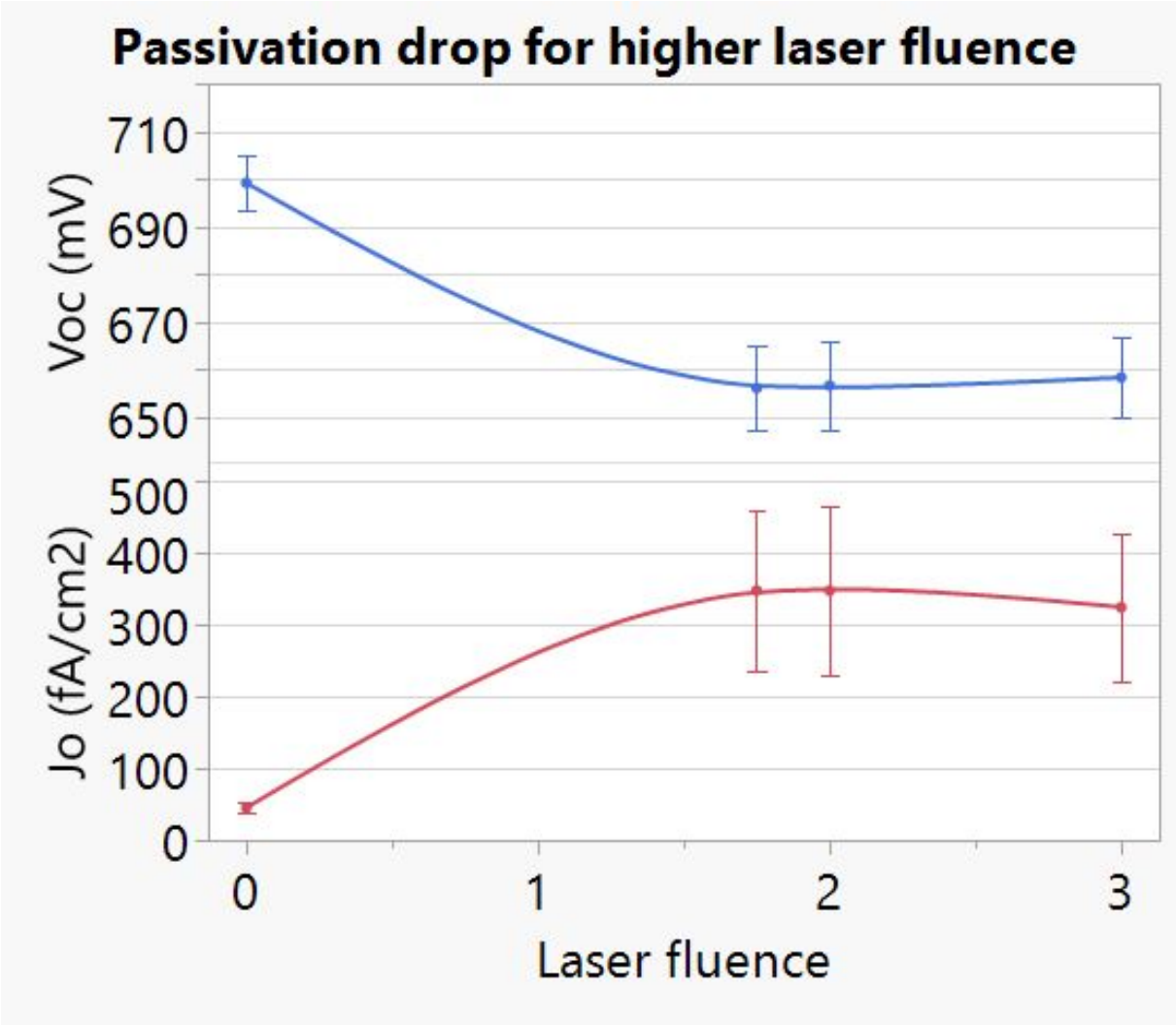

Figure A.2: Lower passivation after high laser power (fluence)

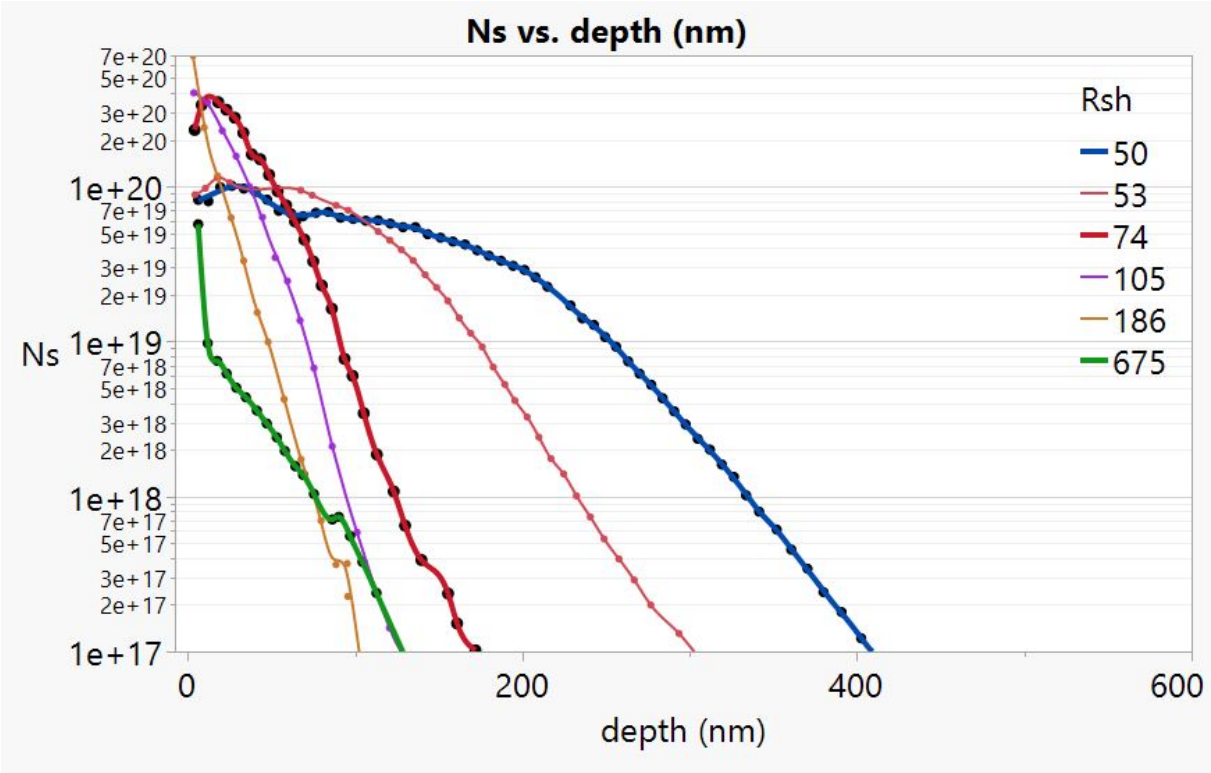

Figure A.3: ECV for all laser settings

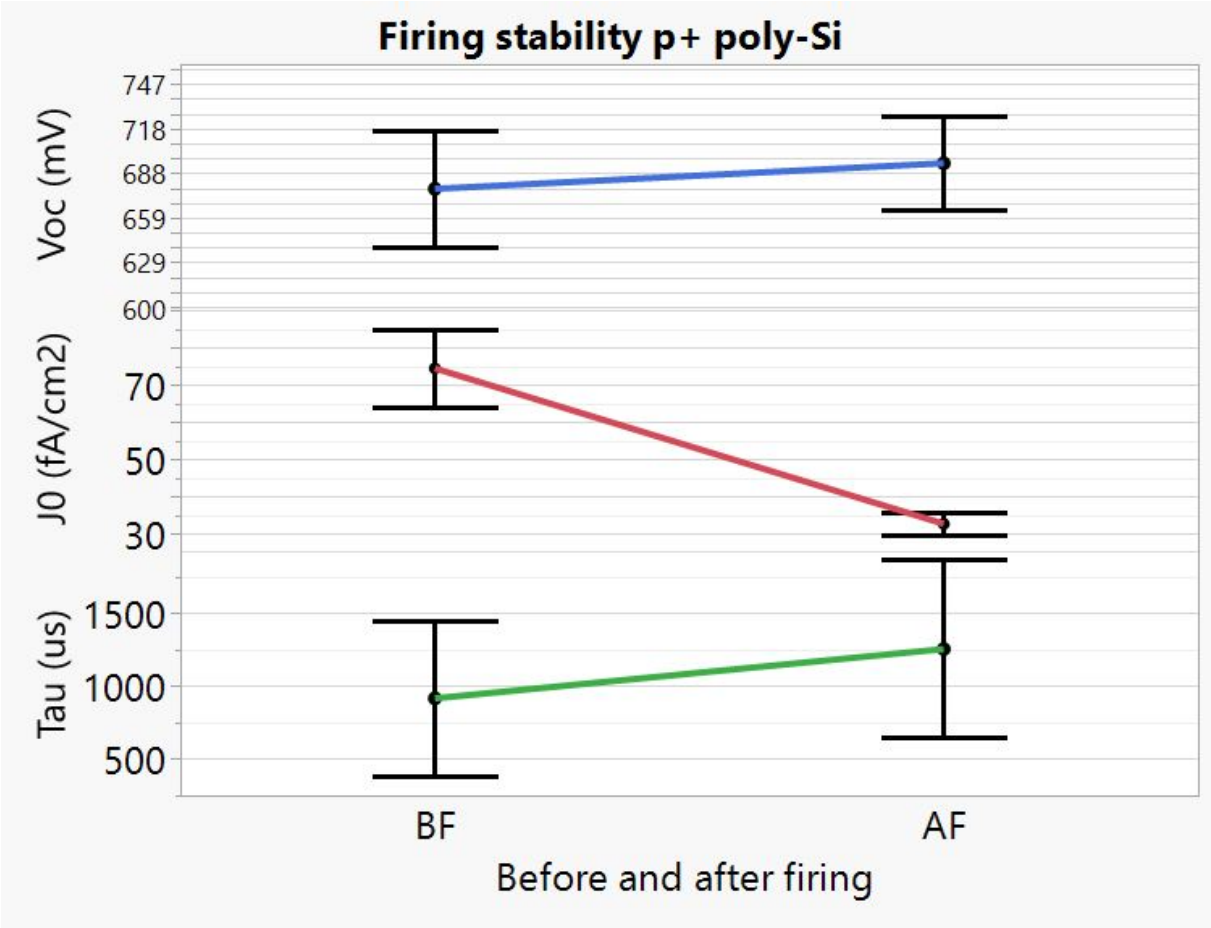

Figure A.4: Firing stability of the poly-Si layer